Pre-Print Copy. Please cite as:
L. Ma & P. Bocchini (2019). Hysteretic model of single-bolted angle connections for lattice steel towers.
Journal of Engineering Mechanics, ASCE, in press, DOI: 10.1061/(ASCE)EM.1943-7889.0001630

HYSTERETIC MODEL OF SINGLE-BOLTED ANGLE CONNECTIONS FOR LATTICE STEEL TOWERS

Liyang Ma, S.M.ASCE[1] and Paolo Bocchini, Ph.D., M.ASCE[2]

[1]Research Assistant. Dpt. of Civil and Environmental Engineering, Lehigh University.
[2]Associate Professor. Department of Civil and Environmental Engineering, Lehigh University. Corresponding author. Email: paolo.bocchini@lehigh.edu

ABSTRACT

Single-Bolted angle joints are widely used on secondary bracings of lattice steel towers due to their low cost and ease of construction. It has been observed that the hysteretic behavior of these joints has significant impact on the dynamic performance of the tower structure and the non-structural components supported by the tower. However, the various phases of this hysteretic cycle were never investigated in detail. Therefore there are no accurate numerical models for this type of joints in the popular software packages for structural analysis. This, in turn, hinders advanced studies on the performance of these critical infrastructure components (utility towers) under strong wind or seismic loads. This paper first explains the mechanics and the various stages of the hysteretic behavior of the joint, including friction, slippage, bolt bearing, and plasticity. Finite element models are built and validated for the analytical modeling of the joint under monotonic loading. The model for hysteretic behavior is then presented, considering cyclic joint slippage and bolt-hole elongation (damage accumulation). A novel algorithm is developed to efficiently incorporate the analytical model into a computer program. In particular, the analytical model is the basis for a new zero-length finite element that can be used in the OpenSees framework. The methodology is applied to single-bolted angle joints with 10 typical configurations. The proposed analytical zero-length element is shown to agree well with brick element simulation results under both monotonic and cyclic loading. Therefore, the hysteretic behavior of the single-bolted angle connections can be incorporated into the dynamic analysis of lattice steel towers by inputting easily obtained physical properties, such as plate thickness and width, bolt and bolt hole diameter, material strength, etc. This proposed element will enable engineers and researchers to efficiently study the cyclic performance of lattice tower structures capturing well the joint behavior.

Keywords: single-bolted connection, hysteretic model, 3D finite element model, joint slippage, lattice steel tower, dynamic analysis.

INTRODUCTION

Lattice steel towers are widely used around the world as power transmission towers to support high voltage electrical transmission lines, and as telecommunication towers to support antennas for telecommunications and broadcasting. The performance of these lattice steel towers during hurricane and seismic events is critical for the power and communication networks. Failures of these towers often result in power and communication loss for days or weeks (NERC 2018). Such lifeline failures not only result in substantial socio-economic loss but also disrupt the recovery process (Hall et al. 1996; Lund 1996; Karamlou and Bocchini 2017).

A lattice steel tower generally consists of steel angle members such as legs, primary and secondary bracings with bearing-type bolted joints connecting these members. Most of these lattice towers in service were designed using linear elastic ideal truss methods, assuming concentric loading and pinned connections. However, full-scale tests have shown that these methods substantially underestimate the lattice tower deflections (Petersen 1962). The discrepancy between the linear elastic truss model results and the experimental results can be attributed to (1) second-order effects of the angle steel members and material nonlinearity; (2) joint effects, including joint eccentricity and joint slippage. The second-order effects of the angle members have been studied extensively. Al-Bermani and Kitipornchai (1992b) utilized finite element analysis to model the angle members in the tower as asymmetrical thin-walled beam-column elements with geometric and material nonlinearity considered. Similarly, a general three-dimensional L section beam element was developed for large deformation analysis by Lee and McClure (2006), considering material and geometric nonlinearities.

The joint effects have also been recognized. Rotational stiffness of the joint can be modeled by zero-length elements with rotational degrees of freedom (Al-Bermani and Kitipornchai 1992a). Kitipornchai et al. (1994) carried out a theoretical study of the bolt slippage and developed static models for typical lattice tower joints. They concluded that the magnitude of the slippage may be as large as the elastic elongation of the connected members. Ungkurapinan et al. (2003) conducted an experimental study to develop empirical mathematical expressions to describe the slip and load-deformation behavior of the joint. Jiang et al. (2011) used these models to carry out the static finite element analysis of a lattice transmission tower and compared it to a full-scale test. The results showed that only the models considering joint slippage were in agreement with the experiential results. They found that the joint slippage dramatically increases the tower deformation and its influence on the tower capacity is relevant, even if it varies in different load cases. Some static experimental tests have been carried out by researchers to study the joint effect (Ahmed et al. 2009; Peng et al. 2015), and it was confirmed that the joint slippage has a significant influence on the tower behavior by reducing its load-carrying capacity, as well as increasing its deflection.

Single-bolted joints are widely used in lattice steel towers connecting the secondary braces. These joints, along with the other types of bolted joints such as two-bolted joints and lap splice joints, contribute to 90% of dynamic energy dissipation of a lattice structure resulting from friction and the slip mechanism (Beards 1992). Therefore, the behavior of these joints has a significant impact on the dynamic performance of a lattice steel tower.

All the mentioned researchers have modeled the joint effects under static loading conditions, but to date no publication has investigated the mechanical model for the hysteretic behavior of single-bolted connections under dynamic loading conditions. Without detailed models of the hysteretic behavior, engineers cannot carry out dynamic simulations of lattice towers considering appropriately the joint effects. In addition, the current state-of-the-art model using empirical mathematical expression is based on one joint configuration (fixed thickness and width), which prevents its application to other joint configurations.

To address these gaps, a hysteretic model for singe-bolted joints is developed and implemented into a computer program. Therefore, the hysteretic behavior of the single-bolted connections can be easily and efficiently incorporated into the dynamic analysis of lattice steel towers. The load-deformation behavior of the joint is modeled analytically and the model is applicable to all typical joint configurations. The research approach consists of three parts and its flowchart is presented in Fig. 1. The first part is to interpret the mechanics and the various phases of the hysteretic behavior. The second part is to build and validate a numerical model based on three-dimensional finite elements, and to develop and validate an analytical model based on the finite element simulation results and fundamental structural mechanics. Then an algorithm is developed to implement the analytical model into a zero-length finite element. The third part is to apply the methodology to the joints with configurations commonly used on lattice towers and compare the cyclic response computed from the developed analytical model with the cyclic response derived from brick element simulations.

MECHANICS OVERVIEW

In order to develop a hysteretic model of single-bolted connections, a preliminary study of its underlying mechanics was conducted to provide a better understanding of the joint hysteretic behavior. The joint hysteresis consists of tensile and compressive loading conditions, and each of these conditions has multiple phases, such as before slippage phase and bolt bearing phase, and each of these phases has multiple force transferring mechanisms activated. As a result of these mechanisms, there are substantial differences between different phases. The aim of this section is to demonstrate the interaction mechanism between plate and bolt and lays a foundation for deriving the analytical representation of the single-bolted connection hysteresis. A schematic of the single-bolted joint hysteresis along with the time history of the applied force and free body diagrams is presented in Fig. 2. The joint has experienced both tension and compression through multiple phases, as indicated in this figure. The mechanisms of these phases are individually described in the following.

"Before slip" is the phase in which the joint behavior is governed by static friction. The applied load is transferred by friction between two contact surfaces: the surface between the upper plate and the lower plate, and the surface between the bolt heads and the plates. Since the friction transfer activates a large area of the plate cross-section, the deformation of the connection during the *"Before slip"* phase can be characterized as a linear elastic elongation of the plate cross-section. The stiffness during this phase is therefore approximated by the axial stiffness of the cross-section.

The *"Slippage"* phase takes place when the applied load reaches the static frictional

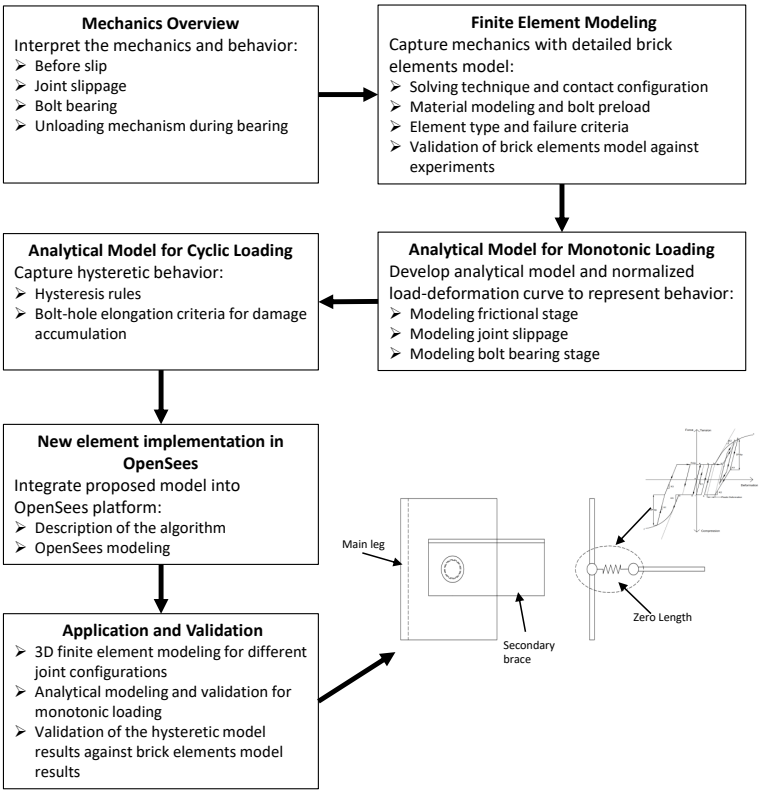

Fig. 1. Flowchart of the research procedure

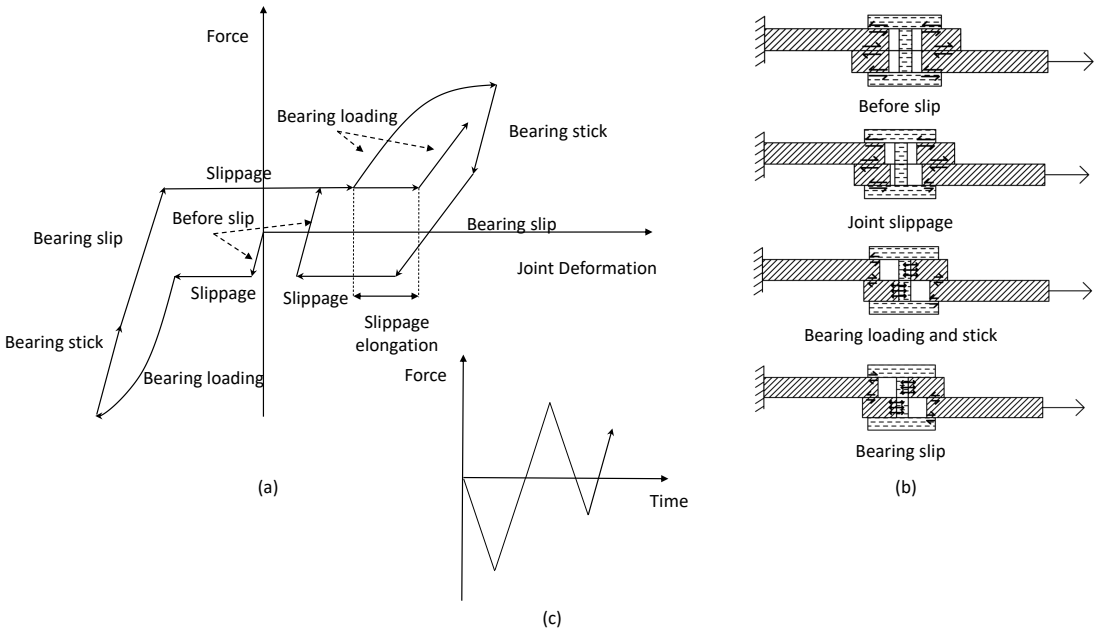

Fig. 2. (a) Joint hysteresis (b) Free-body diagrams of the joint (c) Time history of the load

resistance, which is defined as the threshold force above which the friction can no longer lock the contact surfaces and prevent relative motion between these surfaces. The frictional resistance is proportional to the bolt clamping force and the frictional coefficient of the contact surfaces. During the *"Slippage"* phase, the applied force remains constant and the loading plate moves relatively to the bolt and the other plate in a rigid body motion following the direction of the applied load. Therefore the joint has effectively zero stiffness during the *"Slippage"* phase. In theory, the amount of slip depends on the position of the bolt. However, when multiple hysteretic cycles are considered, the initial position of the bolt becomes practically irrelevant. Hence, for the sake of simplicity, in this study it is assumed that the bolt is initially positioned in the center of the bolt holes of two connection plates. For each plate, the bolt could slip one half of its bolt-hole clearance. Therefore, initially the maximum length of slip is equal to the hole clearance. After the first bearing phase, the maximum length of slip becomes twice the hole clearance plus the bolt-hole elongation. In reality, as reported by some experiential tests, the slip length is often less than the theoretical amount, due to the deviations from the ideal design dimensions of the joint to the real construction (Ungkurapinan et al. 2003).

The *"Bearing loading"* phase begins when the bolt shank comes into direct contact with the plate. During the *"Bearing loading"* phase, the two plates continue moving relatively to each other as the applied load increases. In addition to the friction mechanism, bearing stresses are developed at the contact surfaces between the bolt shank and the plates. The applied load is now transferred through two mechanisms: the friction mechanism, in which the force transferred is equal to the frictional resistance; and the bearing mechanism, through which all the rest of the applied force is transferred. The part of the plate in contact with the bolt shank becomes plastic almost immediately, due to stress concentration, and the bearing area increases with the load, resulting in propagation of material yielding around the bearing area. The joint stiffness during the *"Bearing loading"* phase is much less than that of the *"Before slip"* phase, because of the yielding in the bearing area and a smaller elastic activated area of the plate cross-section. In addition, the bolt and some parts of the plate may develop significant bending and shearing mechanisms, which further decreases the stiffness. At the end of *"Bearing loading"* phase, a large nonlinear deformation is developed and the joint may reach its ultimate capacity with various failure modes depending on the configurations of the joint, which will be discussed later.

When unloading initiates during the *"Bearing loading"* phase, the relative movement between plates stops immediately as the frictional force falls below the frictional resistance. The contact surfaces are therefore locked, and no relative motion is permitted. The joint enters the *"Bearing stick"* phase, in which the relative position of bolt and plates remains unchanged from the *"Bearing loading"* phase. Without relative movement between bolt and plates, the bearing deformation cannot be recovered, and the bearing force transferred between the bolt shank and the plate remains unchanged. Therefore, the reducing load is balanced solely by the reduction of the frictional force. Because of the inactive bearing mechanism during this phase, the friction mechanism dominates, and the decrease of the joint deformation is due to the linear elastic recovery of the plate cross-section. Thus, the stiffness of the joint in this phase can be well

approximated by that of the *"Before slip"* phase.

The *"Bearing stick"* phase continues until the unloading force overcomes the frictional resistance in the opposite direction. The contact surfaces are no longer locked and plates are free to move relatively, but in the opposite direction from the first loading. The joint enters the *"Bearing slip"* phase. The Frictional force remains equal to the frictional resistance in this phase, while the deformed bearing part of the plate starts to recover, and the bearing force begins to decrease. The bearing mechanism dominates this phase, thus the stiffness of this phase is larger than that of the *"Bearing stick"* phase. During the *"Bearing slip"* phase, the bolt shank is being gradually pushed away from the bearing part of the plate. When the bolt shank finally detaches from the bearing part of the plate, the joint will reenter the *"Slippage"* phase.

The nonlinear deformation in the *"Bearing loading"* phase causes a permanent bolt-hole elongation. This elongation can be accumulated throughout loading cycles and resulting in larger slippage.

RECOMMENDED PROTOCOL FOR FINITE ELEMENT MODELING AND FAILURE MODES

A numerical model based on solid-mechanics three-dimensional brick element model is developed using ABAQUS (Hibbit et al. 2012) to study the joint behavior. A major challenge consists in modeling correctly the bolt slip process, in which the bolt moves as a rigid body. Special care needs to be taken in selecting and setting the parameters of the numerical solver and of the contact configuration to prevent numerical divergence during the analysis, as explained below. Also, failure modes observed in experimental tests need to be captured by the finite element model.

It is well known that models containing contact problems are computationally expensive and often make the convergence extremely difficult, due to numerical instability. Some researchers recommend an explicit solution scheme, due to its ease with contact problems and the fact that it is usually associated with very small increments, which in turn helps also convergence (Van der Vegte and Makino 2004). However, the implicit method outperforms the explicit method in better predicting the deformation during bearing when the bearing region becomes close to fully plastic, while explicit formulation often times renders an unrealistic deformation of the bearing region (Sekanet and Garlock 2010). Therefore, an implicit solution scheme with quasi-static load application and displacement control is used in this research. The 'NLGEOM' option is adopted in ABAQUS to model the geometric nonlinearities of the connection. Contact surfaces are illustrated in Fig. 3. ABAQUS uses a contact algorithm to check for open or closed nodes on contact surfaces. If the slave nodes are open, it means that they are not in contact with the master nodes, thus they are unconstrained. To determine the tangential behavior of the closed slave nodes (sliding or sticking), the equivalent shear stress is calculated and compared with the critical shear stress, which is computed by multiplying contact force by the coefficient of friction. For galvanized joints, the coefficient of friction is reported to be equal to 0.153 (Kennedy 1972). To enforce contact constraint, the penalty method is selected due to its higher convergence rate (Sekanet and Garlock 2010). The finite sliding method is chosen as the contact tracking algorithm, because it is well suited for connection models with large movement between surfaces.

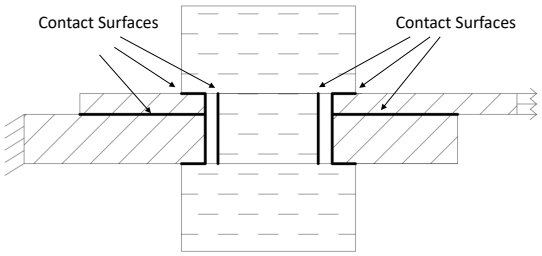

Fig. 3. Contact surfaces defined in the finite element model

The stress-strain curves of steel plates are recommended to be simulated by the kinematic hardening model. The engineering stress-strain values are converted to true stress and true strain to be used in the finite element models. The bolt preload is simulated using the BOLT LOAD option in ABAQUS. The bolt load is defined on the cross-section of the bolt shank through the axis perpendicular to the cross section, and the bolt is positioned in the center of the bolt-hole with uniform clearance. The washers are not modeled, due to their small relative movement, which has little impact on joint deformation (Oldfield et al. 2005). The 8-node linear brick with incompatible modes (C3D8I) element has superior performance in bending problems at relatively low computational expense, and thus it is recommended for modeling the plate section under compression. The C3D8R (reduced integration) elements can be used to decrease the computational expense, however they are not suited for contact and bending mechanisms. Thus, C3D8R elements are used outside of the contact region and bending region. The plate flange to which the load is applied is under large bending moment, especially near the bolt hole region where stress concentration occurs, while the bending moment for the other flange is relatively small. Therefore, the loaded angle flange is recommended to have three elements through its thickness, while the other flange needs only one element through the plate thickness. For the bolt-hole region, a mesh of at least 24 elements around the circumference is suggested (Bursi and Jaspart 1998).

For the boundary conditions of this model, the outstanding flange of the plate to which the loaded plate is connected is set to be fixed, while the end of loaded flange of the loaded plate are supported by springs along the edge. These springs are intended to model the edge support from the rest of the secondary brace, which is not included in this joint model. The angle plate acts as a short column in compression, which is prone to torsional-flexural buckling due to its low torsional stiffness compared to its flexural stiffness. These springs simulate the support provided by the rest of the secondary brace to resist the local torsional buckling of the loaded flange. Without these springs, unrealistic early torsional buckling of the joint model may occur, which might result in the underestimation of the compressive capacity of the joint. The springs provide support in the lateral and out-of-plane directions, and the stiffness is approximated with classical bending stiffness as:

$$K_{spring} = \frac{3EI}{NL_{total}{}^3} \tag{1}$$

where E is the Young's modulus of the loaded secondary brace. I is the moment of inertia of the plate cross-section. L_{total} is the total length of the loaded secondary brace, and N is the number of springs, which is set to be 6 for this study. The ASI (2007) gives the following expression for the slenderness ratio for torsional-flexural buckling:

$$\lambda_{TF} = \frac{5.3w}{t} \tag{2}$$

where w is the width of the plate and t is the thickness of the plate. This slenderness ratio represents an approximation of the maximum critical value of slenderness above which weak-axis flexural buckling dominates. In other words, if the slenderness of the brace plate is larger than λ_{TF}, global flexural buckling of the plate will happen before joint failure. Because of the focus of the research is joint failure, the total length of the secondary brace is set to be:

$$L_{total} = \frac{\lambda_{TF} r}{K} \tag{3}$$

Where r is the radius of gyration for the weak axis of the brace plate and K is the column effective length factor, equal to 1 for single-bolted joints. For braces whose length is larger than L_{total}, the global flexural buckling occurs before joint failure. For braces whose length are smaller than L_{total}, they are prone to inelastic buckling and their buckling capacities are not sensitive to the brace length. Therefore, L_{total} is a good modeling choice to investigate the joint.

Five failure modes are identified: bolt shear failure, local buckling, bearing failure, shear rupture and net section failure. Bolt shear failure is a brittle failure in which the material exhibits little ductility before the fracture occurs (Kulak et al. 1987). In single-bolted joints, the load is transferred between the connected plates by shear across the bolt cross section. The bolt shear failure is deemed to have occurred when the shear load in the bolt exceeds its shear capacity. Bolt failure is not modeled explicitly in the brick element model, but it is included in the analytical model and zero-length element implementation.

Local buckling behavior is observed both in tension and compression. Curling is one type of local buckling behavior that happens in tension and is described as the plate below the bolt buckling out of the original plane (Rex and Easterling 2003). In compression, the loaded angle flange is prone to buckling due to secondary bending, which can be described by a bending moment resulting from the eccentric load applied to the joint (Zhao et al. 2016). Local buckling is deemed to have occurred when a clear peak from the load-deformation curve is observed from the finite element simulations.

Since there is no agreement on the bearing failure based on deformation criteria (Rex and Easterling 1996), it is here defined based on a strength criterion. In this study, it is assumed that the bearing failure occurs when the maximum load capacity is reached in the finite element simulations.

Unlike local buckling and bearing failure, whose peak load might be identified as the ultimate capacity in the finite element simulations, shear rupture and net section failure usually do not have such clear peaks, if fracture propagation is not included in the finite element model. In this study, these failure modes are modeled based on the fracture strain criterion (Salih et al. 2010), so that the fracture propagation modeling can

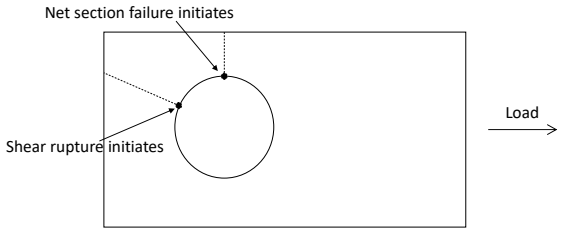

Fig. 4. Shear rupture and net section failure

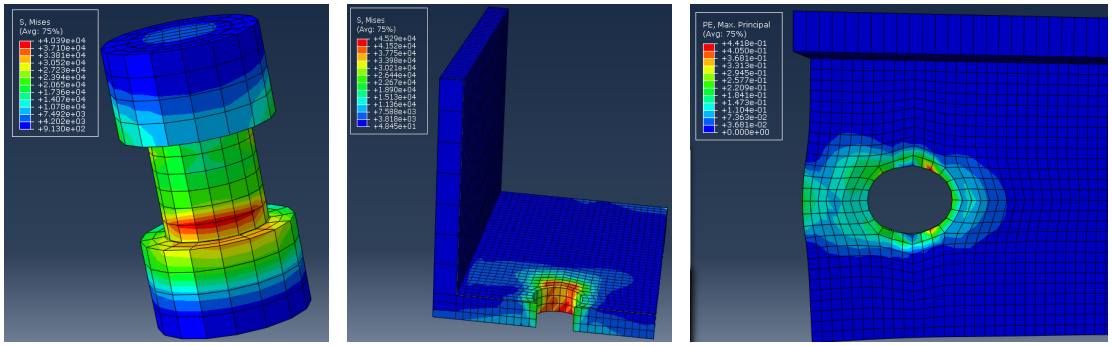

(a) (b) (c)

Fig. 5. Finite element analysis results: (a) stress distribution of the bolt shank; (b) stress distribution of the bolt hole; (c) plastic deformation of the bolt hole

be avoided. The value of localized fracture strain for structural steel is considered to be equal to 100% based on several experimental investigations (Khoo et al. 2000). Thus, when the plastic strain magnitude (PEMAG) reaches the fracture strain of 100%, a crack is assumed to initiate, and the failure is considered to occur. The fracture is expected to develop in the bolt-hole region, where large stress concentration occurs. Shear rupture and net section failure can be distinguished by the location where the fracture initiates, as showed in Fig. 4. After initiation, the crack propagates in the direction illustrated by the dashed line.

Some results of the finite element analysis are provided in Fig. 5. In particular, the stress distribution over the contact areas of the bolt shank and bolt-hole are depicted in Figs. 5(a) and 5(b), respectively. Fig. 5(c) shows the plastic deformation of the bolt-hole.

The finite element models are validated against experimental results in two steps. In the first step, a brick element model is built to reproduce the test done by Ungkurapinan (2000) and shown in Fig. 6. Joint slippage from the finite element simulation is in good agreement with the test results. The amount of slippage predicted by finite element model is larger than the test results, which confirms what mentioned in previous section. The discrepancy between the finite element simulation and the test lays in the bearing behavior. The finite element model has a substantially larger value of initial bearing stiffness than the test, and it might be the result of boundary conditions which are not described with sufficient details in the test. To validate the bearing behavior,

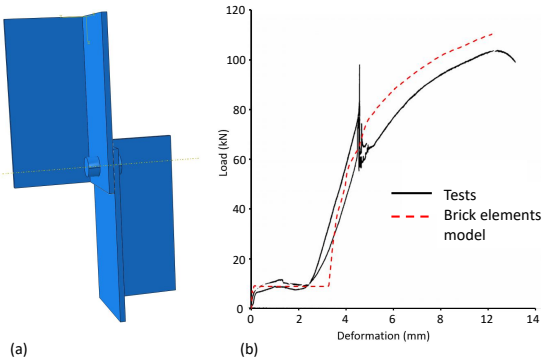

Fig. 6. (a) Brick elements model of the test; (b) Comparison of the load-deformation curves

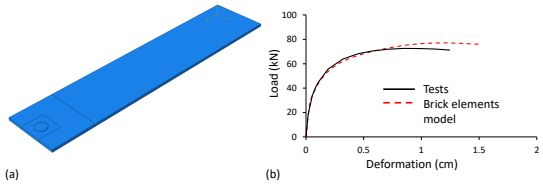

Fig. 7. (a) Brick elements model of the test; (b) Comparison of the load-deformation curves

another finite element model is built to validate against a test done in Virginia Tech (Rex and Easterling 1996). Even though this test is conducted on a single-plate single-bolted connection, without considering slippage, it is sufficient for validating bolt-plate bearing behavior. The test and numerical results are in good agreement, as demonstrated in Fig. 7. It can be concluded that the developed brick element model is capable of simulating the joint behavior with good accuracy, therefore, it can be employed as reference for the hysteretic and parametric analysis for the joint.

ANALYTICAL MODEL FOR MONOTONIC LOADING

This section presents an analytical method to predict the load-deformation behavior of a single-bolted joint under monotonic loading conditions. The load-deformation curve and its parameters are shown in Fig. 8. The joint monotonic behavior is composed of compressive loading and tensile loading, and each case consists of three phases: *"Before slip"*, *"Slippage"* and *"Bearing loading"*. All the parameters required to construct the load-deformation curve are derived in this section. Since the *"Bearing loading"* phase has a nonlinear load-deformation curve, a nonlinear analytical expression developed by Richard and Elsalti (1991) is used herein.

The deformation of the connection during the *"Before slip"* phase can be characterized as linear elastic elongation of the plate cross section. The stiffness during this phase under both tension and compression is therefore approximated by the axial stiffness K_{eb} of the effective cross-section:

$$K_{eb} = \frac{A_{eff}E}{L_{eff}} \tag{4}$$

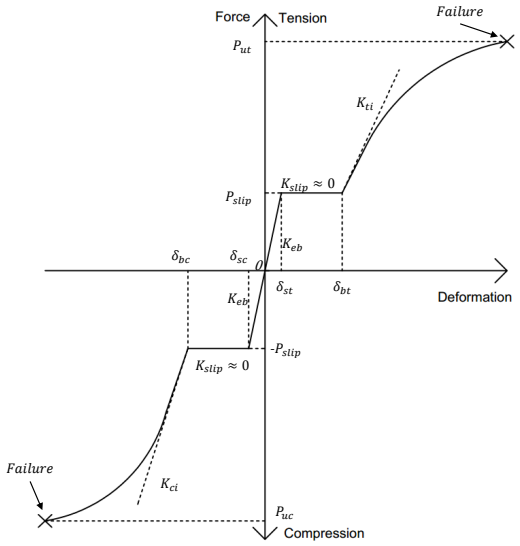

Fig. 8. Load-deformation curve of the joint under monotonic loading

where E is the Young's modulus of the the brace angle plate. A_{eff} is the effective cross-section of the plate, and it can be computed as one half of the net cross-sectional area A_n shown in Fig. 9:

$$A_n = wt + (w - t)t \tag{5}$$

$$A_{eff} = \frac{A_n}{2} \tag{6}$$

L_{eff} is the effective length shown in Fig. 9, which is determined as the distance required for the stress distribution become uniform in the plate:

$$L_{eff} = \frac{w + (w - t)/2}{\tan\theta} \tag{7}$$

where $\theta = 30^o$ is the angle of the spread force specified according to the Eurocodes (CEN 2005). When slippage occurs, the applied force is equal to the frictional resistance P_{slip}, and it can be determined using the formula (Kulak et al. 1987):

$$P_{slip} = \mu m P \tag{8}$$

where μ is the coefficient of friction, m is the number of slip planes and P is the bolt clamping force.

The *"Slippage"* phase can be characterized as a plateau, starting from δ_{st} to δ_{bt} for tension and from δ_{sc} to δ_{bc} for compression. The length of the slippage plateau equals to the construction clearance by assuming the bolt positioned at the center of the bolt hole.

The *"Bearing loading"* phases of the joint under tension and compression are different due to different mechanisms and failure modes. The *initial bearing stiffness of joint under compression* is the combination of the bearing stiffness of two connecting

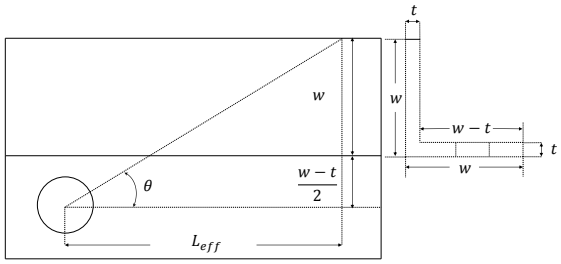

Fig. 9. Effective length and angle of the spread force

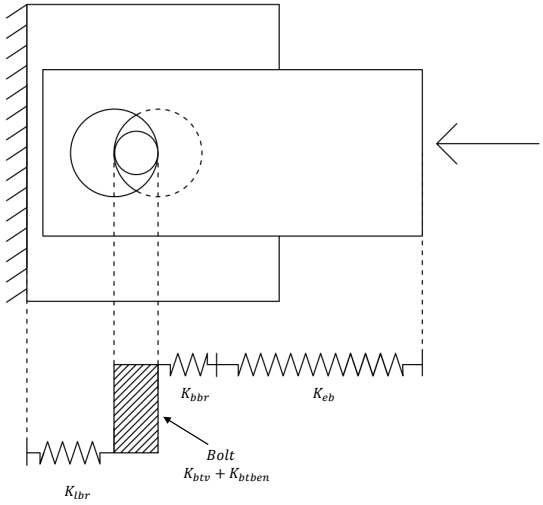

Fig. 10. Initial stiffness of the joint in compression

plates (K_{bbr} and K_{lbr}), the elastic stiffness of the plate to which the load is applied (K_{eb}), bending (K_{btben}) and shear (K_{btv}) stiffness of the bolt as shown in Fig. 10. The initial stiffness of the joint under compression is calculated putting all the mentioned components in series:

$$K_{ci} = \frac{1}{\frac{1}{K_{bbr}} + \frac{1}{K_{lbr}} + \frac{1}{K_{eb}} + \frac{1}{K_{btben}} + \frac{1}{K_{btv}}} \tag{9}$$

the bearing stiffness for the two connecting plates can be computed as (Rex and Easterling 2003):

$$K_{bbr} = 120 t F_y d_b \tag{10}$$

$$K_{lbr} = 120 t_l F_{yl} d_b \tag{11}$$

where t and t_l are the thickness of the two connecting plates, F_y and F_{yl} are the yielding strength of the two plates, and d_b is the bolt diameter. Shear and bending stiffness of the bolt are derived using the classical equations:

$$K_{btben} = \frac{3 E_{bt} I_{bt}}{(t + t_l)^3} \tag{12}$$

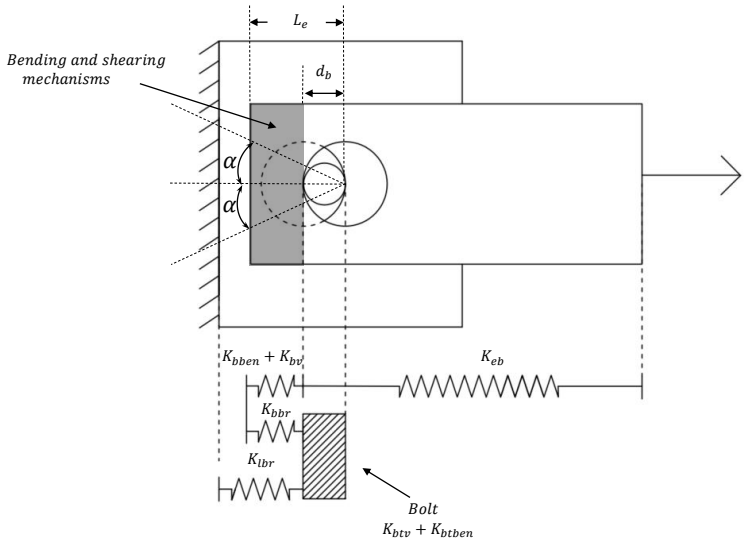

Fig. 11. Initial stiffness of the joint in tension

$$K_{btv} = \frac{32}{37}\left(\frac{G_{bt}A_{bt}}{t + t_l}\right) \tag{13}$$

where A_{bt} is the circular area of the bolt, and I_{bt} is the moment of inertia of the circular area. E_{bt} is the elastic modulus of the bolt, and G_{bt} is the shear modulus of the bolt.

The mechanisms which contribute to the *initial bearing stiffness of the joint under tension* are indicated in Fig. 11. In addition to the bearing deformation and bolt deformation which are the same as the joint under compression, the bearing loading phase of the joint under tension also activates the bending and shearing mechanisms in the part of the plate highlighted in Fig. 11. This part of the plate, between the bolt and the edge, behaves like a rectangular elastic fixed end beam. The bending (K_{bben}) and shearing (K_{bv}) stiffness of the beam are (Rex and Easterling 2003):

$$K_{bben} = 32\ E_{bt}t\left(L_e - \frac{d_b}{2}\right)^3 \tag{14}$$

$$K_{bv} = 6.67\ G_{bt}t\left(L_e - \frac{d_b}{2}\right) \tag{15}$$

where L_e is the distance between the center of the bolt hole and the free edge. Therefore, the initial bearing stiffness of the joint under tension (K_{ti}) can be computed as:

$$K_{ti} = \frac{1}{\frac{1}{K_{ci}} + \frac{1}{K_{bben}} + \frac{1}{K_{bv}}} \tag{16}$$

where K_{ci} is the initial bearing stiffness of the joint under compression.

The failure modes for the joint under compression are either bearing failure at the bolt-hole or local buckling failure of the plate. Therefore, the *joint capacity under*

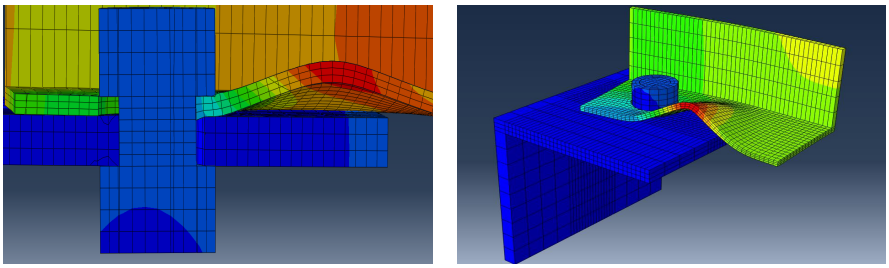

Fig. 12. Local buckling of the joint

compression is taken as the minimum of the two failure capacities. The bearing strength (R_{nbr}) is determined as suggested by AISC (2011):

$$R_{nbr} = 2.4\ d_b t F_u \tag{17}$$

where t is the plate thickness and F_u is the ultimate strength of the steel. Local buckling of the joint, as shown in Fig. 12, is initiated by the small angle rotation of the plate caused by excessive hole clearance and deformation of the bolt. For typical angle sections listed in AISC (2011), because of their small width-to-thickness ratio, the elastic buckling capacity of the flange is considerably larger than its yielding strength. Therefore, the local buckling is initiated by the inelastic deformation of the flange and the local buckling strength (R_{nbk}) can be approximated by the yield strength of the flange (Timoshenko and Gere 2009):

$$R_{nbk} = A_f F_y \tag{18}$$

where A_f is the cross-sectional area of the flange. When local buckling occurs, the flange buckles out of the original plane resulting in large torsion and causes the whole plate to fail in torsional-flexural buckling. Three modes of failure are possible for the joint in tension, which are net section failure, bearing failure and shear rupture. The *joint capacity under tension* is taken as the minimum of these three failure capacities. The net section failure strength (R_{net}) is computed from equation (AISC 2011):

$$R_{net} = A_{net} F_u \tag{19}$$

where

$$A_{net} = (w - d_b)t \tag{20}$$

All the existing strength model treat bearing and shear rupture failures as one limit state (Rex and Easterling 2003). Therefore, one strength values is provided for both failure modes. One of the most common strength model for predicting bearing failure and shear rupture was developed by Fisher and Struik (1974):

$$R_{nv} = 0.7\ F_u A_{nv} \tag{21}$$

where A_{nv} is the net area subject to shear. It can be determined by two shearing planes which radiate from the edge of the bolt to the end of the plate at an angle α as shown in

Fig. 11:

$$A_{nv} = \frac{2t\left(L_e - \frac{d_b}{2}\right)}{\cos\alpha} \tag{22}$$

In this research, α is taken as 30^o as suggested by the Eurocodes (CEN 2005). Shear strength of the bolt can be determined from equation (AISC 2011):

$$R_{nbt} = F_{nvbt} A_b \tag{23}$$

where A_{bt} is the nominal unthreaded body area of bolt or threaded part, and F_{nvbt} is the shear strength of the bolt.

A normalized load-deformation behavior is chosen to represent the *"Bearing loading"* phase of the joint. To develop the normalized behavior, load-deformation data for different joint configurations were collected by conducting finite element simulations. Then, to remove the effects of different joint configurations, the load was normalized by the maximum load capacity and the displacement was normalized by the ratio of the load capacity over the initial stiffness (Rex and Easterling 1996). A continuous nonlinear expression developed by Richard and Elsalti (1991), usually called "Richard equation", is utilized to represent the highly nonlinear bearing behavior of the joint, as shown in Eq. (24). Fig. 13 shows the nonlinear equation along with the parameters required to complete the expression. Each parameter has its physical meaning, which is aligned with the approach preferred in this research. A nonlinear regression analysis is conducted to determine the parameters of the Richard equation:

$$\frac{R}{R_n} = \frac{\bar{\Delta} K_1}{\left[1 + \left(\frac{\bar{\Delta} K_1}{R_0}\right)^n\right]^{1/n}} + \bar{\Delta} K_p \tag{24}$$

where R is the plate load; R_n is the strength of the joint determined from analytical model; R_0 is the reference load determined by regression analysis; $\bar{\Delta}$ is the normalized deformation is the $\Delta K_i / R_n$; Δ is the deformation; K_i is the initial stiffness determined from analytical model; K_p is the reference stiffness determined by regression analysis; K_1=K_i-K_p; and n is the curvature parameter determined by regression analysis.

ANALYTICAL MODEL FOR CYCLIC LOADING AND DAMAGE ACCUMULATION

An analytical model for single-bolted joints hysteresis considering bolt slippage and damage accumulation, was developed and is presented in this section. The response of the joint under cyclic loading is presented as hysteresis loops in Fig. 14. The load-deformation behavior depends not only on the instantaneous deformation, but also on the response history. The backbone curve (*o-a-b-c* for tension and *o-d-e-f* for compression) of the hysteresis loops is derived based on the analytical model under monotonic loading presented in the previous section.

If the hysteresis loop occurs before bearing, as indicated by loop *h-q-i* in Fig. 14, then the joint follows the load-deformation behavior of a perfectly plastic material.

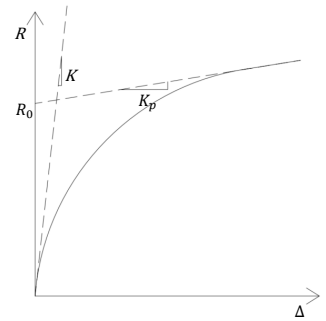

Fig. 13. Nonlinear expression of the *"Bearing loading"* behavior, Richard equation

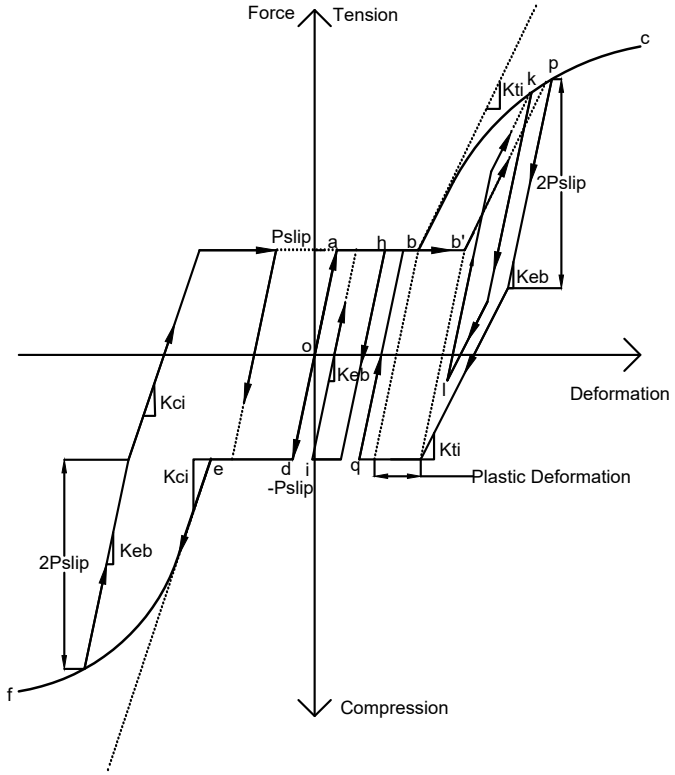

Fig. 14. Hysteresis loops of the joint under cyclic loading

Loading and unloading stiffness are both K_{eb}, which is the axial stiffness of the effective cross-section. Once the applied force reaches the frictional resistance P_{slip}, the force remains constant and the joint is in *"Slippage"* phase until unloading, or until reaching points *b* or *e* where the *"Bearing loading"* phase begins.

The hysteresis rules of the joint during *unloading* from bearing follows a bilinear behavior because it consists of two phases: *"Bearing stick"* and *"Bearing slip* as introduced in the previous section. Once unloading initiates at points *p* or *k*, the joint is in the *"Bearing stick"* phase in which the unloading stiffness is K_{eb}. Since the frictional force falls below the frictional resistance, there is no relative displacement between the bolt and bearing part of the plate in this phase, and the reduced deformation of the

joint in this phase is due to the recovery of the axial linear deformation of the plate cross-section. When the joint unloads twice the frictional resistance ($2P_{slip}$), the joint enters the *"Bearing slip"* phase, in which the bolt is able to disengage from the bearing part of the plate. Therefore, the bearing force starts to decrease, while the frictional force remains constant. The stiffness of this phase reflecting the recovery of the bearing deformation is defined by the initial bearing loading stiffness: K_{ti} for unloading from tension and K_{ci} for unloading from compression.

The hysteresis rules of the joint during *reloading* need to be considered separately for two conditions: the joint reloads before slippage, as shown in the cycle k-i in Fig. 14; or the joint reloads after slippage, as in the cycle p-q. For the first case, when the joint reloads from point l and enters the *"Bearing stick"* phase there is no relative movement between the bolt and the bearing part of the plate, and thus no additional bearing deformation occurs in this phase. The reloading stiffness is K_{eb} until the joint reloads twice the frictional resistance ($2P_{slip}$). Then, the reloading stiffness becomes K_{ti} for tension and K_{ci} for compression, reflecting the additional bearing deformation in this phase. For the second case, when the joint reloads from point q during slippage as shown in Fig. 14, it first overcomes the frictional resistance and then starts to slip in the opposite direction. Because of the plastic bearing deformation at point p, the bolt-hole is permanently elongated. Therefore, the joint enters bearing at point b' instead of point b. The bearing follows a linear load-deformation behavior with the initial bearing stiffness, until it reaches the backbone curve.

Cyclic responses of the single-bolted joints exhibit *damage accumulation (permanent bolt-hole elongation)* causing additional bolt slippage. This bolt-hole elongation is attributed to the plastic deformation of the plate during the bolt bearing process in tension and compression. The bolt-hole elongation can be quantified from the joint plastic deformation described in Fig. 14. The joint plastic deformation can be obtained in the cyclic responses analysis, however, it not only consists of the bolt-hole elongation but also consists of the cross-section plastic deformation, which should not be counted as the damage accumulation for slippage assessment purposes. As illustrated in Fig. 15, the permanent bolt-hole elongation is represented by the elongation between points C and B, while the plastic deformation for sections DC and BA should be excluded. In tension, the bolt-hole elongation between points C and B constitutes most of the plastic deformation of the plate, and the plastic deformation for sections DC and BA are relatively small. While in compression, the plastic deformation for section BA also contributes to the total plastic deformation. The quantitative measure of the permanent bolt-hole elongation is conducted by finite element simulations. From the simulations, approximately 80% of the plastic deformation in tension and 60% of the plastic deformation in compression should be attributed to the permanent bolt-hole elongation.

The permanent bolt-hole elongation results in increase of maximum slip length. The new maximum slip length is given by the summation of the original maximum slip length and the permanent bolt-hole elongation. As illustrated in Fig. 16, the joint has been loaded in tension and undergoes large plastic bearing deformation. Since only part of the plastic deformation can be attributed to permanent bolt-hole elongation, point e, which is the original point of bearing initiation in compression, has to be moved to point e'. Thus, after nonlinear bearing deformation, the backbone curve needs to be updated

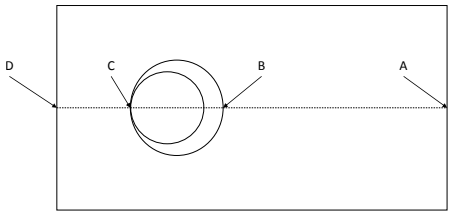

Fig. 15. Different sections of the plate for considerations on damage accumulation

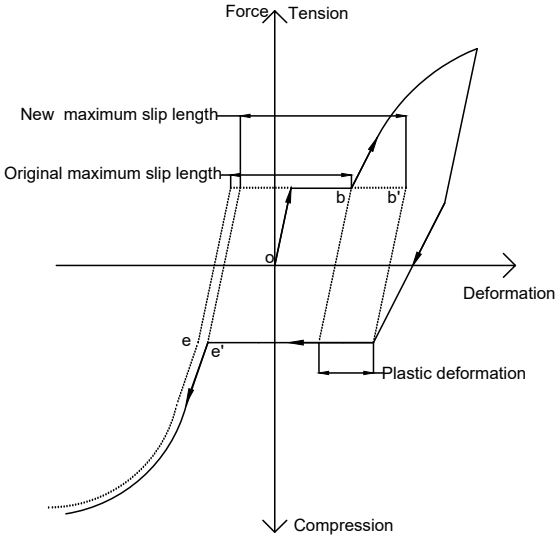

Fig. 16. Rules for update of maximum slip length and backbone curve due to damage accumulation

to take into account the new maximum slip length.

ZERO-LENGTH JOINT ELEMENT FORMULATION AND IMPLEMENTATION

The reference FE model based on brick elements is computationally too complex to be effectively incorporated in a lattice tower model with dozens of joints. Thus, a novel OpenSees UniaxialMaterial is developed on the basis of the described analytical model. The computer code of this material has been programmed in two versions: Matlab (for development and debugging) and C++ (for subsequent compilation). Source code for both versions can be accessed from a repository on GitHub (Ma and Bocchini 2018), for use and further improvements from the scientific community. This material is implemented into a zero-length element for the OpenSees platform. This element captures the joint response under dynamic loading conditions considering the joint slippage and the damage accumulation with good accuracy. With a few input parameters describing the joint configuration and material properties, analysts can subject the joint element to any cyclic time history loadings, and compute the joint response with great computational efficiency.

The required input variables are the geometric and material properties of the joint.

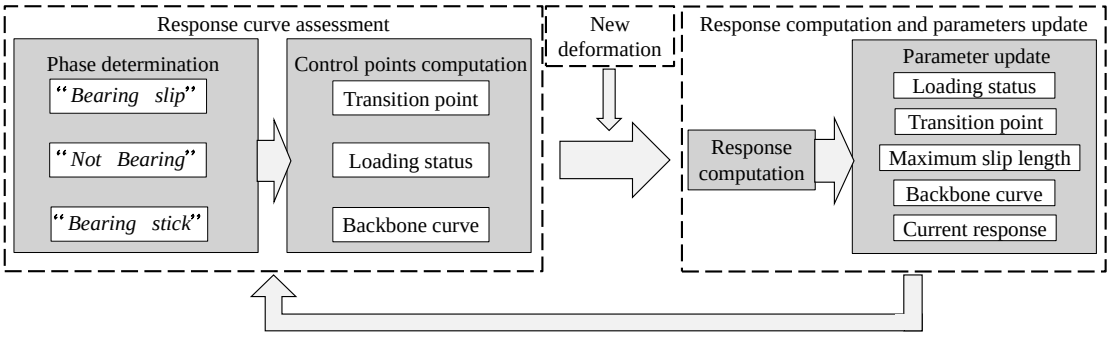

Fig. 17. Algorithm of the OpenSees UniaxialMaterial implementation

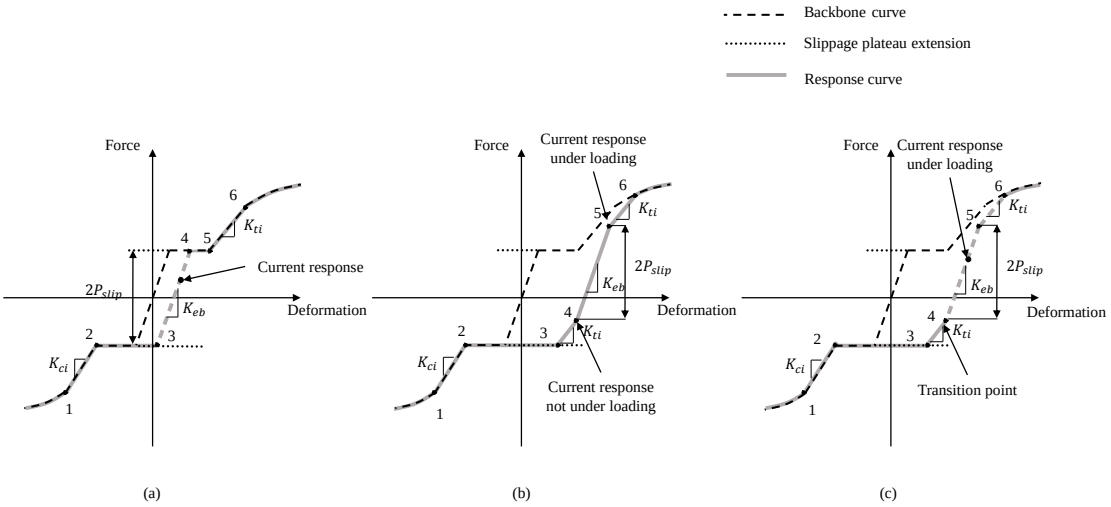

Fig. 18. Control points determination in three conditions: (a) Not bearing (b) Bearing slip (c) Bearing stick

Based on the these, the joint stiffness in the different phases is computed using the equations introduced in the previous sections. In addition, the backbone curve that describes the monotonic behavior of the joint is established and stored for the subsequent time history analysis.

The computation of the joint response subjected to cyclic loading conditions is based on the construction of a response curve at every time step. The response curve includes the current response and all the possible responses at next time step. The joint response can be computed by getting the force on the response curve corresponding to the new joint deformation. To establish the response curve, six control points are required, as shown in Fig. 18. Each control point indicates change of stiffness and joint load-deformation phases in the response curve. The control points are determined by the current phase of the joint and the updated backbone curve.

If the current phase of the joint is *"Not bearing"*, and the current response is given, then the control points can be computed as shown in Fig. 18(a). In particular, control points 4 and 3 are determined by intersecting a straight line with stiffness K_{eb} with

the backbone curve and its slippage plateau extension. The rest of the control points overlap with the backbone curve: control points 5 and 2 are where the bearing initiates in tension and compression, respectively; control points 6 and 1 are the transitions from linear bearing behavior to nonlinear bearing behavior represented by Richard equation.

If the joint is in the *"Bearing slip"* phase, the loading status is required to determine the control points 4 and 5, as shown in Fig. 18(b). If the joint is currently under (increasing) loading, control point 5 is equal to the current response. To reach control point 4 which is in the unloading path, twice the frictional resistance force ($2P_{slip}$) has to be overcome. If the joint is not under loading, control point 4 equals the current response, and control point 5 has force $2P_{slip}$ larger than control point 4.

When the joint is in the *"Bearing stick"* phase, in which the joint is in the process of overcoming the frictional force, in addition to the loading status, a transition point is required to determine the control points. The transition point is essentially the point where the most recent load direction change happened. For example, if the joint is currently under loading, control point 4 should be equal to the transition point shown in Fig. 18(c). If the joint is not currently under loading, control point 5 is equal to the transition point. Once control point 4 or 5 has been determined, the rest of the control points can be derived accordingly.

With the six control points, the response curve can be determined. The force response in the next time step can be computed by using the force on the response curve corresponding to the new deformation input. The parameters of the joint should be updated accordingly in every time step.

The proposed algorithm was implemented in MATLAB (2016) first, for simplicity and validation purposes. Then, it has been re-implemented in C++ and formulated as a novel zero-length element for the OpenSees (Mazzoni et al. 2006) platform.

APPLICATION AND VALIDATION

The methodology for developing the hysteretic model of single-bolted joints was applied to 10 typical joint configurations. The joints feature 10 different sizes of the secondary brace members, as shown in Table 1, which are commonly used in lattice steel towers. The main leg members to which the secondary brace member is connected is assumed to be made of an equal angle plate with width equal to 101.6 millimeters (4 inches) and thickness equal to 7.9375 millimeters (5/16 inches), which is one of the most typical sizes of main leg members in lattice steel towers. The schematic representation of the joint configuration is illustrated in Fig 19. The typical end distance $E1$ is 25.4 millimeters (1 inch), and $E2$ equals to $(w - t)/2$. The bolt diameter d_b is 15.875 millimeters (5/8 inches), and hole diameter D is equal to 17.4625 millimeters (11/16 inches), which is 1.5875 millimeters (1/16 inches) larger than the bolt diameter. The length of the secondary brace considered in the joint (L) is determined as the distance from the edge of the plate to the part of the plate where the stress distribution becomes uniform, as described in a previous section. The bolt is pretensioned by a torque T = 113.9 N-M, consistent with the tests done by Ungkurapinan (2000). The clamping force P is calculated as:

$$P = \frac{T}{K_{torque} d_b} \tag{25}$$

where K_{torque} is the torque coefficient, which can range from 0.10 for a well lubricated/waxed assembly, to over 0.30 for one that is dirty or rusty. In this research, K_{torque} is assumed to take the typical value 0.25.

The material properties used in this study are listed in Table 2. The reference brick element models are developed using ABAQUS, as shown in Fig. 20. The models are subjected to monotonic loading first. A comparison of the force-deformation behavior along with steel plate failures (bolt failure excluded) of different joint configurations is presented in Fig 21. The behaviors before bearing are almost the same, but the bearing capacities are quite different among different joint configurations. Table 3 compares the compressive and tensile strength considering steel plate failure obtained from the ten brick element models with those obtained from the proposed algorithm. The ratios of the brick element strength to the zero-length element strength for different configurations of joints are between 1.00 and 1.04 under tension and between 0.92 and 1.12 under compression. Therefore, it is evident that the zero-length element can predict the joint compressive and tensile strength with good accuracy.

The load-deformation behaviors of various joints derived from finite element simulations are used to compute the parameters of the Richard equation. The capacity and initial stiffness used to normalize the load-deformation curves are computed using the developed analytical methods. Then, a nonlinear regression is conducted to determine the parameters for the Richard equation. The resulting values for compression and tension are given in Table 4. The capability of the proposed zero-length element to predict the load-deformation behavior of the joints under monotonic loading condition is assessed by comparing the zero-length element results to the ABAQUS finite element simulation results, as shown in Fig 22. It is observed from the figure that zero-length element is able to predict the joint monotonic behavior with good accuracy.

The quantification of bolt-hole elongation is conducted by using numerical simulation. It is concluded that approximately 80% of the plastic deformation in tension and 60% of the plastic deformation in compression contributes to the bolt-hole elongation. The input parameters are the frictional resistance, as well as the geometrical and material properties of the two connecting plates and bolt. Comparisons of the load-deformation behaviors under cyclic loading derived from the ABAQUS finite element model and the zero-length element are shown in Fig. 23. The hysteretic responses derived from zero-length element are in good agreement with the results obtained from ABAQUS finite element simulations. Therefore, the proposed element can be used to evaluate the cyclical performance of lattice transmission towers built with single-bolted joint. To compute the time history response for one joint configuration in Fig. 23, using the ABAQUS finite element model takes 12 hours in average on a desktop PC with an Intel Core i7-6700 quad-core processor and 16 GB of RAM . However, the zero-length element is able to derive the time history response in less than 1 second. Therefore, significant computational time can be saved for engineers and researchers when computing multiple single-bolted joint hysteretic behaviors in full lattice tower analyses.

CONCLUSIONS

This paper presents a methodology to analyze efficiently and accurately the dynamic behavior of single-bolted joints, which are critical connections in popular structures. The

Configurations	Width unit:mm (inches)	Thickness unit:mm (inches)
1	50.8 (2)	3.2 (1/8)
2	50.8 (2)	4.8 (3/16)
3	50.8 (2)	6.4 (1/4)
4	50.8 (2)	7.9 (5/16)
5	63.5 (2 1/2)	4.8 (3/16)
6	63.5 (2 1/2)	6.4 (1/4)
7	63.5 (2 1/2)	7.9 (5/16)
8	76.2 (3)	4.8 (3/16)
9	76.2 (3)	6.4 (1/4)
10	76.2 (3)	7.9 (5/16)

Table 1. Typical sizes of secondary brace members

	Secondary brace (A36)	Main leg (High strength steel)
Young's modulus	200000 MPa (E)	200000 MPa
Yield strength	250 MPa (F_y)	345 MPa (F_{yl})
Poisson Ratio	0.26	0.3
Ultimate strength	415 MPa (F_u)	485 MPa
Ultimate strain	0.2	0.2

Table 2. Summary of the material properties

Configurations	Compressive strength (kN)			Tensile strength (kN)		
	Numerical	Analytical	Ratio	Numerical	Analytical	Ratio
1	36.77	40.03	0.92	35.38	35.39	1.00
2	62.05	60.05	1.03	52.84	53.09	1.00
3	89.99	80.07	1.12	72.37	70.79	1.02
4	111.69	100.08	1.12	89.10	88.48	1.01
5	69.79	75.06	0.93	54.54	53.09	1.03
6	97.59	100.08	0.98	71.75	70.79	1.01
7	118.99	125.11	0.95	88.65	88.48	1.00
8	76.06	75.06	1.01	55.29	53.09	1.04
9	105.96	100.08	1.06	72.55	70.79	1.02
10	124.02	125.11	0.99	90.39	88.48	1.02

Table 3. Comparison of strength between numerical and analytical models

Parameters	Compression	Tension
K_1	7.289	4.568
K_p	-0.0071	0.0137
R_0	2.775	1.046
n	0.330	0.493

Table 4. Richard equation parameters

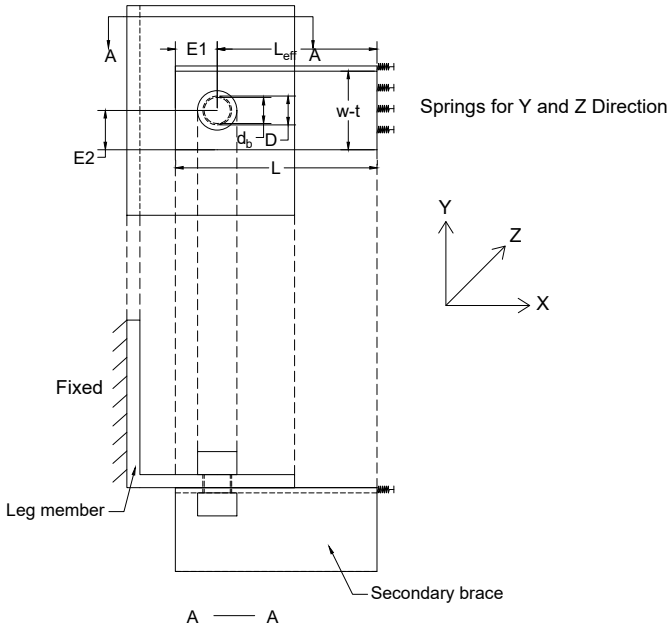

Fig. 19. Schematic of the joint model

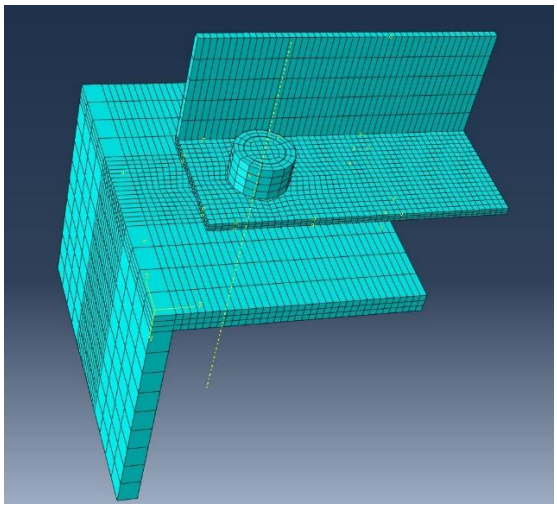

Fig. 20. 3D finite element model of the joint

proposed methodology has been validated against experimental results and numerical tests. For single-bolted angle connections, analysts can directly implement the developed OpenSees material (Ma and Bocchini 2018) into zero-length elements to model joints, with the parameters provided in Table 4. For single-bolted connections of different types, the analysts have to follow the protocol described in the paper to find the appropriate parameters of the Richard equation, and then they can use such parameters in the same OpenSees material.

A detailed joint model with brick finite elements has been developed and validated against monotonic load tests available in the literature. In the model development,

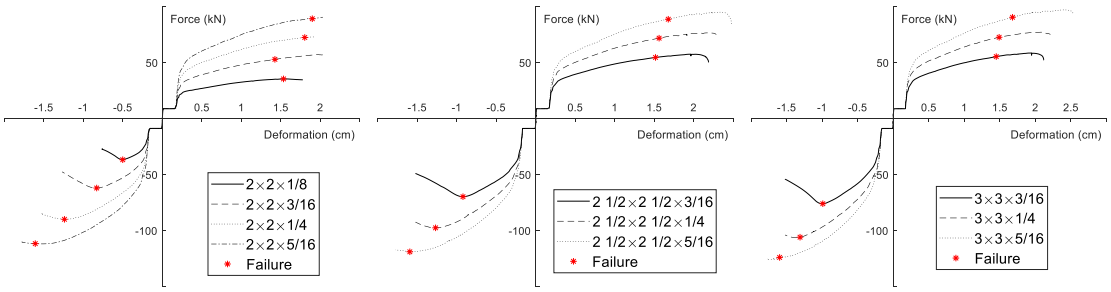

Fig. 21. Numerical simulations of load-deformation behaviors for joints with different configurations

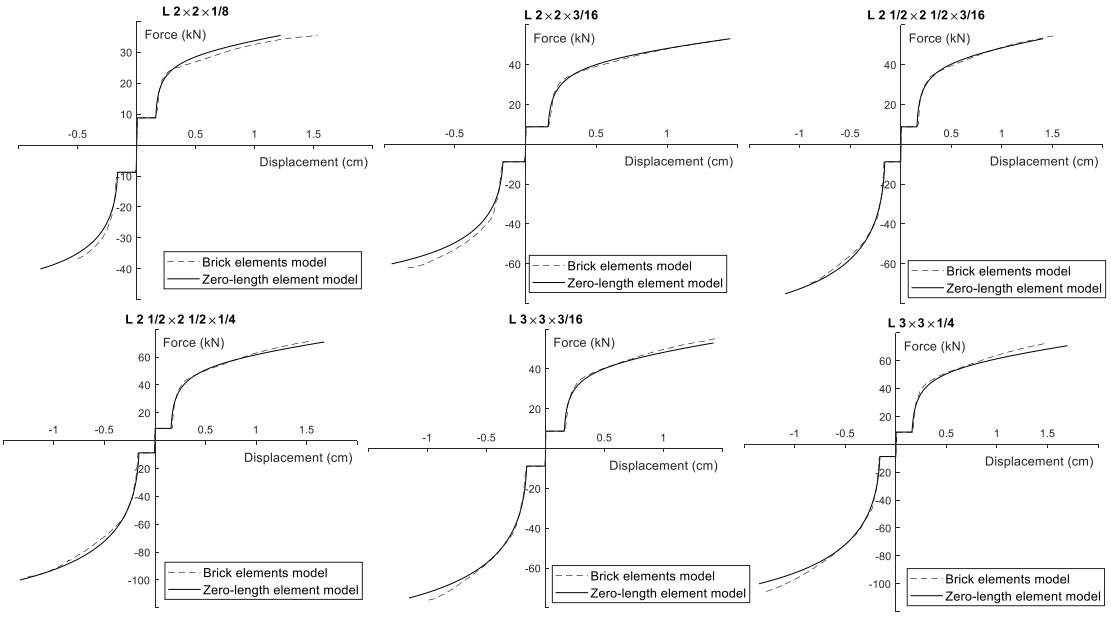

Fig. 22. Comparison between numerical and analytical joint behaviors with different configurations under monotonic loading

special emphasis is given on failure criteria and boundary conditions. A fracture strain criterion is used to predict the failure modes of shear rupture and net section failure for the joint. To correctly capture the compressive strength, this paper proposes to use spring elements to model the edge boundary conditions, with stiffness determined by the total length of the secondary brace and the moment of inertia of the cross-section. This model is then used as reference to investigate the complex hysteretic behavior of the joint.

In particular, five main phases of the load-deformation behavior are identified, and specific methods are developed to describe analytically each phase. To model the nonlinear bearing behavior, initial bearing stiffness and load capacity are computed analytically. Parameters for the Richard equation are derived using ABAQUS simulations and nonlinear regressions. Hysteresis rules are established, and a bolt-hole elongation criterion is introduced to capture the damage accumulation during cyclic loading.

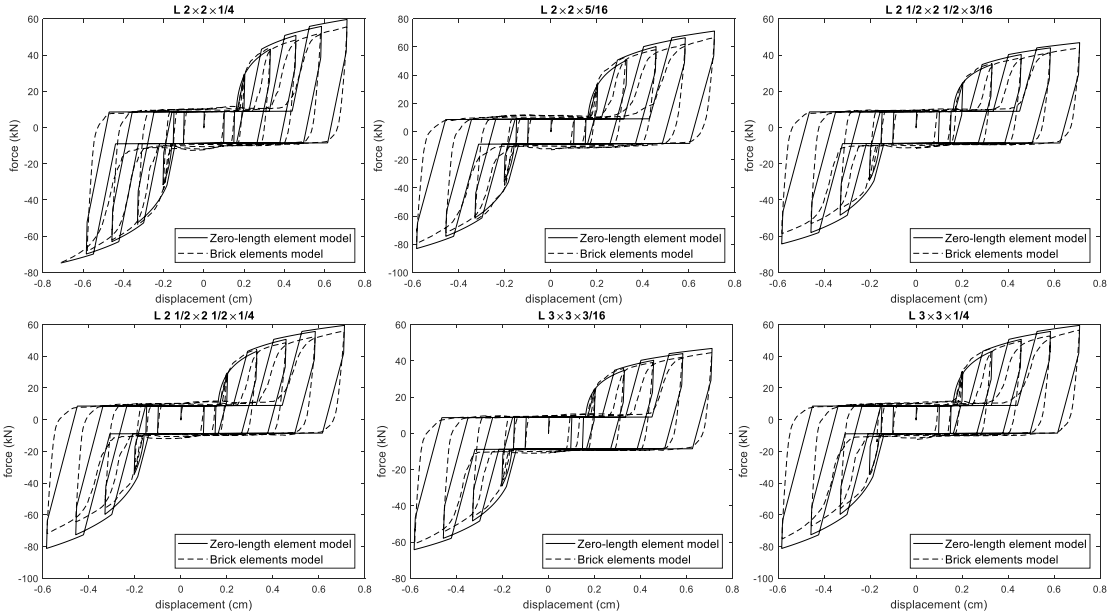

Fig. 23. Comparison between numerical and analytical joint behaviors with different configurations under cyclic loading

A novel algorithm is developed to efficiently incorporate this mechanical behavior into a zero-length element for the OpenSees platform. The element is capable of modeling large nonlinear deformation, joint slippage and damage accumulation under cyclic loading conditions. Therefore, it can be applied to seismic and wind dynamic analyses for lattice tower structures. The responses of the zero-length element subjected to cyclic loadings agree well with the responses obtained from the brick elements model simulations.

The insight on bolted connection mechanics and the new finite element publicly shared with the community will allow engineers and researchers to efficiently study the cyclic performance of lattice tower structures considering the joint hysteretic behavior with good accuracy. Further developments of this study may include an analytical model for joints with multiple bolts. Such extension will require to consider the situation in which some bolts are in bearing mode and some are slipping, generalize the mechanical model accordingly, and therefore update the Finite Element models. Also, self-loosening and preload loss mechanisms of the bolt could be incorporated into the hysteretic model. The effect of uncertainties in construction and joint properties needs further investigation to provide a probabilistic evaluation for the joint behavior.

ACKNOWLEDGMENTS

This work is part of the “Probabilistic Resilience Assessment of Interdependent Systems (PRAISys)” project (www.praisys.org). The support from the National Science Foundation through grant CMS-1541177 is gratefully acknowledged.

The opinions and conclusions presented in this paper are those of the authors and do not necessarily reflect the views of the sponsoring organizations.

REFERENCES

Ahmed, K. I. E., Rajapakse, R. K. N. D., and Gadala, M. S. (2009). "Influence of Bolted-Joint Slippage on the Response of Transmission Towers Subjected to Frost-Heave." *Advances in Structural Engineering*, 12(1), 1–17.

AISC (2011). "Manual of Steel Construction." *Report No. 14th Edition*, CHICAGO, IL.

Al-Bermani, F. G. A. and Kitipornchai, S. (1992a). "Elastoplastic Nonlinear Analysis of Flexibly Jointed Space Frames." *Journal of Structural Engineering*, 118(1), 108–127.

Al-Bermani, F. G. A. and Kitipornchai, S. (1992b). "Nonlinear analysis of transmission towers." *Engineering Structures*, 14(3), 139–151.

ASI (2007). "1-1: Eurocode 2-design of concrete structures-part 1-1: General rules and rules for buildings-national specifications concerning önorm en 1992-1-1, national comments and national supplements." *Austrian Standards Institute, Vienna*.

Beards, C. (1992). "Damping in structural joints." *The Shock and Vibration Digest*, 24(7), 3–7.

Bursi, O. S. and Jaspart, J. P. (1998). "Basic issues in the finite element simulation of extended end plate connections." *Computers & Structures*, 69(3), 361–382.

CEN, E. (2005). "1-1-eurocode 3: Design of steel structures-part 1-1: General rules and rules for buildings." *European Committee for Standardization, Brussels*.

Fisher, J. W. and Struik, J. H. A. (1974). *Guide to Design Criteria for Bolted and Riveted Joints*. wiley Interscience.

Hall, J., Holmes, W., and Somers, P. (1996). "Northridge Earthquake of January 17, 1994: Reconnaissance Report, Volume 1." *Report no.*, Earthquake Engineering Research Institute, Oakland, CA.

Hibbit, H., Karlsson, B., and Sorensen, E. (2012). "Abaqus user manual, version 6.12." *Simulia, Providence, RI*.

Jiang, W. Q., Wang, Z. Q., McClure, G., Wang, G. L., and Geng, J. D. (2011). "Accurate modeling of joint effects in lattice transmission towers." *Engineering Structures*, 33(5), 1817–1827.

Karamlou, A. and Bocchini, P. (2017). "Functionality-fragility surfaces." *Earthquake Engineering & Structural Dynamics*, 46(10), 1687–1709.

Kennedy, D. J. L. (1972). "High Strength Bolted Galvanized Joints." *Journal of the Structural Division*, 98(12), 2723–2738.

Khoo, H., Cheng, R., and Hrudey, T. (2000). "Ductile fracture of steel. structural engineering report no. 233." *Report no.*, Department of Civil and Environmental Engineering, University of Alberta.

Kitipornchai, S., Al?Bermani, F., and Peyrot, A. (1994). "Effect of Bolt Slippage on Ultimate Behavior of Lattice Structures." *Journal of Structural Engineering*, 120(8), 2281–2287.

Kulak, G. L., Fisher, J. W., and Struik, J. H. A. (1987). *Guide to Design Criteria for Bolted and Riveted Joints, 2nd Edition*. Wiley-Interscience, New York, 2 edition edition (March).

Lee, P.-S. and McClure, G. (2006). "A general three-dimensional L-section beam finite element for elastoplastic large deformation analysis." *Computers & Structures*, 84(3), 215–229.

Lund, L. (1996). "Lifeline utilities performance in the 17 January 1994 northridge, California, Earthquake, Bulletin of the Seismological Society of America." *Report No. 86(1B)*.

Ma, L. and Bocchini, P. (2018). "Opensees material for single-bolted connection." *Computer code, Lehigh University*, DOI:10.5281/zenodo.1308074.

MATLAB (2016). *version 9.1 (R2016b)*. The MathWorks Inc., Natick, Massachusetts.

Mazzoni, S., McKenna, F., Scott, M. H., and Fenves, G. L. (2006). "The open system for earthquake engineering simulation (opensees) user command-language manual.

NERC (2018). "Hurricane Harvey event analysis report." *Report no.*, North American Electric Reliability Corporation.

Oldfield, M., Ouyang, H., and Mottershead, J. E. (2005). "Simplified models of bolted joints under harmonic loading." *Computers & Structures*, 84(1), 25–33.

Peng, W., Hui-wu, Z., Xing, Z., and Min, Y. E. (2015). "Effect of bolt joint on the behaviour of transmission tower with non-uniform settlement." *Engineering Mechanics*, 32(10), 209–219.

Petersen, W. O. (1962). "Design of EHV Steel Tower Transmission Lines." *Journal of the Power Division*, 88(1), 39–66.

Rex, C. O. and Easterling, W. S. (1996). "Behavior and Modeling of A Single Plate Bearing on A Single Bolt." *Report No. CE/VPI-ST 96/14*, Virginia Polytechnic Institute and State University, Structures and Materials Research Laboratory (November).

Rex, C. O. and Easterling, W. S. (2003). "Behavior and Modeling of a Bolt Bearing on a Single Plate." *Journal of Structural Engineering*, 129(6), 792–800.

Richard and Elsalti (1991). "PRCONN, Moment-Rotation Curves for Partially Restrained Connections. Users manual for program developed at The Univ. of Arizona, Dept. of Civil Engineering and Engineering Mechanics." *Report no.*, Tucson, Arizona.

Salih, E. L., Gardner, L., and Nethercot, D. A. (2010). "Numerical investigation of net section failure in stainless steel bolted connections." *Journal of Constructional Steel Research*, 66(12), 1455–1466.

Sekanet, S. and Garlock, M. (2010). "Guidelines for modeling three dimensional structural connection models using finite element methods." Istanbul, Turkey (September).

Timoshenko, S. P. and Gere, J. M. (2009). *Theory of Elastic Stability*. Dover Publications, Mineola, N.Y, 2nd ed. edition edition (June).

Ungkurapinan, N. (2000). "A Study of Joint Slip in Galvanized Bolted Angle Connections." Ph.D. thesis, University of Manitoba, Winnipeg, Manitoba (April).

Ungkurapinan, N., Chandrakeerthy, S. R. D. S., Rajapakse, R. K. N. D., and Yue, S. B. (2003). "Joint slip in steel electric transmission towers." *Engineering Structures*, 25(6), 779–788.

Van der Vegte, G. and Makino, Y. (2004). "Numerical simulations of bolted connections: The implicit versus the explicit approach." *Connections in Steel Structures*, 5.

Zhao, L., Xin, A., Liu, F., Zhang, J., and Hu, N. (2016). "Secondary bending effects in progressively damaged single-lap, single-bolt composite joints." *Results in Physics*, 6, 704–711.